Continuous Role Adaptation for Human–Robot Shared Control

Yanan Li, *Member, IEEE*, Keng Peng Tee, *Member, IEEE*, Wei Liang Chan, Rui Yan, *Member, IEEE*, Yuanwei Chua, and Dilip Kumar Limbu

***Abstract*—In this paper, we propose a role adaptation method for human–robot shared control. Game theory is employed for fundamental analysis of this two-agent system. An adaptation law is developed such that the robot is able to adjust its own role according to the human's intention to lead or follow, which is inferred through the measured interaction force. In the absence of human interaction forces, the adaptive scheme allows the robot to take the lead and complete the task by itself. On the other hand, when the human persistently exerts strong forces that signal an unambiguous intent to lead, the robot yields and becomes the follower. Additionally, the full spectrum of mixed roles between these extreme scenarios is afforded by continuous online update of the control that is shared between both agents. Theoretical analysis shows that the resulting shared control is optimal with respect to a two-agent coordination game. Experimental results illustrate better overall performance, in terms of both error and effort, compared with fixed-role interactions.**

***Index Terms*—Adaptive control, physical human-robot interaction, shared control.**

I. Introduction

HUMAN–ROBOT shared control is an emerging research field with many applications such as robotic rehabilitation [1], search and rescue [2], and tele-operation [3]. Humans and robots have complementary capabilities, and their collaboration is a necessity in many situations [4]. In particular, a robot is able to perform a task autonomously with a desired trajectory prescribed based on the rough knowledge about the workpiece, environment, and process, while the human may provide on-task corrective action, fine tuning control, and situational guidance to the robot. This is useful for high-mix low-volume manufacturing where it is not cost-effective to determine accurately the desired robot trajectory corresponding to each workpiece variant. Unfortunately, it is generally difficult to design a good human–robot interface since multiple factors like stability, safety, and usability need to be addressed together [5]. It is also very challenging to apply techniques from multirobot collaboration (e.g., [6] and [7]) to scenarios in which humans are in the loop, because these techniques are not designed to accommodate the unpredictability and unmeasurable uncertainties introduced by humans [8].

The traditional approach of dealing with physical human–robot interaction typically involves the robot yielding compliantly to the motion of the human through an impedance or admittance controller [9]. Subsequently, more sophisticated methods in estimating and recognizing human intention (see, e.g., [10] and [11]) have been developed to provide more cues for the robot to react to, but the control philosophy remains the same, namely, human as leader and robot as follower. The rationale for fixing the roles distinctly is that humans have better cognitive abilities, such as situational awareness and decision-making skills, while robots have better physical abilities, such as precision and strength. However, to require the human to always lead the task and drive the robot means subjecting the human constantly to a high cognitive load, which degrades performance over a prolonged operation. Although specialized applications such as robotic surgery [12] and assistive exoskeletons [13] can benefit from such a fixed-role leader–follower paradigm, the same may not be true in general for other applications. A case in point is cooperative welding [14], where it was shown to be advantageous for a robot to lead during the welding process because the information required to control welding can be obtained more accurately by the robot. Another example is obstacle avoidance, where it is useful for the robot to take over the lead and automatically modify the human-intended motion when it senses an impending collision or safety constraint violation [15]–[17].

The importance of adjustable leader/follower roles for shared control has been emphasized in a recent review [18], and there are several works in this direction. In [19], the role of the robot was switched between leader or follower based on online estimates of impedance parameters that indicate human intention. In [20], a homotopy switching model allowed the behavior of the robot to be adjusted between leader and follower roles in two-agent haptic collaborative tasks. An example of how such tuning can be achieved in practice was given in [21]. A thorough formal analysis of human–robot cooperative load transport was presented in [22], and constructive dynamic role assignment was shown to be advantageous over a static one. It required that a shared plan in the form of a desired trajectory, as well as the common goal of the cooperation task, be known to both agents. In [23], the possibility that the human diverges from the robot's assumed final configuration or path to the goal was considered, and an adaptation strategy was developed to switch between model-based and model-free predictions based on risk-sensitive optimal feedback control [24]. In [25], role adaptation was achieved by adaptive attitude design depending on the disagreement level and the environmental situation, and

Manuscript received November 30, 2014; revised February 22, 2015; accepted April 1, 2015. Date of publication April 28, 2015; date of current version June 3, 2015. This paper was recommended for publication by Associate Editor V. Kyrki and Editor A. Kheddar upon evaluation of the reviewers' comments. This work was supported by the Science and Engineering Research Council, A*STAR, Singapore under Grant 1225100001.

The authors are with the Institute for Infocomm Research, Agency for Science, Technology and Research (A*STAR), Singapore 138632 (e-mail: liy@i2r.a-star.edu.sg; kptee@i2r.a-star.edu.sg; chanwl@i2r.a-star.edu.sg; ryan@i2r.a-star.edu.sg; ychua@i2r.a-star.edu.sg; dklimbu@i2r.a-star.edu.sg).

Color versions of one or more of the figures in this paper are available online at http://ieeexplore.ieee.org.

Digital Object Identifier 10.1109/TRO.2015.2419873

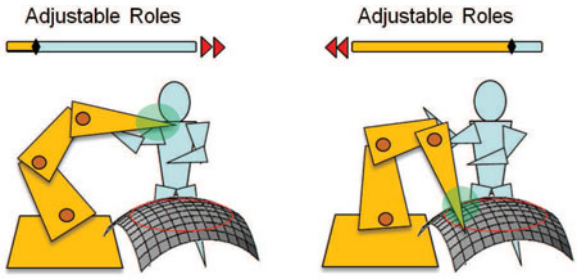

Fig. 1. Illustration of an example scenario of human–robot shared control with adjustable roles.

the possibility of using game theory for the modeling of attitude negotiation between two partners was suggested. As discussed in [26], game theory provides useful tools to analyze complex interactive behaviors involving multiple agents.

In this paper, we employ game theory to analyze human–robot interactive behavior, and develop a framework to make on-the-fly adjustment of the robot's role across a continuous scale between a leader and follower, with the human's goal unknown to the robot. We propose an adaptation law that automatically adjusts the role of the robot, according to the measured interaction force, in order to achieve human–robot coordination. It is important to emphasize that this role adaptation is continuous and not a discrete switching between different states. Moreover, it does not require the human and the robot to share a common goal known to both agents.

The remainder of this paper is organized as follows. In Section II, the human–robot shared control problem is formulated as a two-agent game based on game theory. In Section III, an adaptation law is developed to achieve the human–robot coordination, and its performance is theoretically analyzed. In Section IV, the validity of the proposed method is verified through experimental studies. The limitation of the proposed method and possible future works are discussed in Section V. Section VI concludes this work.

II. Human–Robot Shared Control as a Two-Agent Game

Definition 1: The term "role" is defined as the behavioral pattern that an agent (human/robot) takes on due to a certain shared control scheme [22], and it will be shown to be directly related to the balance of the control input contributed by each agent (human/robot).

We consider an example scenario as illustrated in Fig. 1, where a robot collaborates with a human to perform a task on a workpiece. In this shared control scenario, when the robot end-effector is away from the workpiece, the human should be allowed to take the lead and have the flexibility to preempt or react to unexpected problems, especially in unstructured environments. On the other hand, when the end-effector is near the workpiece, it is desired for the robot to take the lead, since the robot is able to sense the workpiece more accurately and perform the task more precisely. Note that although we illustrate a kinesthetic interaction scenario, the proposed method can also be applied to a teleoperation scenario.

A. Dynamic Model

The forward kinematics of a robot are described by $x(t) = \phi(q(t))$, where $x(t) \in \mathbb{R}^m$ and $q(t) \in \mathbb{R}^n$ are positions in the Cartesian space and in the joint space, respectively. Differentiating it with respect to time leads to $\dot{x}(t) = J(q(t))\dot{q}(t)$, where $J(q(t)) \in \mathbb{R}^{m\times n}$ is the Jacobian matrix. The dynamics of the robot in the joint space are

$$\begin{aligned} &M(q(t))\ddot{q}(t) + C(q(t), \dot{q}(t))\dot{q}(t) + G(q(t)) \\ &= \tau(t) + J^T(q(t))f(t) \end{aligned} \tag{1}$$

where $M(q(t)) \in \mathbb{R}^{n\times n}$ is the inertia matrix, $C(q(t), \dot{q}(t))\dot{q}(t) \in \mathbb{R}^n$ the Coriolis and centrifugal forces, $G(q(t)) \in \mathbb{R}^n$ the gravitational force, $\tau(t) \in \mathbb{R}^n$ the control input, and $f(t) \in \mathbb{R}^n$ the interaction force in the Cartesian space.

We adopt the two-loop impedance control, which includes an inner position control loop and an outer loop [27]. As state-of-the-art robots have controllers that provide very accurate joint position control, we assume a perfect inner position control loop, i.e., $q(t) = q_r(t)$, where $q_r(t)$ is the reference position in the joint space. The outer loop is used to generate $q_r(t)$ according to the following impedance model in the Cartesian space

$$M_d\ddot{x}_r(t) + C_d\dot{x}_r(t) = u(t) + f(t) \tag{2}$$

where $M_d \in \mathbb{R}^{m\times m}$ and $C_d \in \mathbb{R}^{m\times m}$ are given inertial and damping matrices, respectively, $u(t) \in \mathbb{R}^m$ the control input in the Cartesian space, and $x_r(t) \in \mathbb{R}^m$ the reference position in the Cartesian space. By designing $u(t)$ and measuring $f(t)$, the reference velocity in the joint space is obtained based on inverse kinematics, i.e.,

$$\dot{q}_r(t) = J^{\dagger}(q)\dot{x}_r(t) \tag{3}$$

where $J^{\dagger}(q)$ is the pseudoinverse of the Jacobian matrix $J(q)$. Based on the above assumption of a perfect inner position control loop, we have

$$M_d\ddot{x}(t) + C_d\dot{x}(t) = u(t) + f(t). \tag{4}$$

From (4), we see that the two sources $u(t)$ and $f(t)$ are sharing control of the robot.

For ease of analysis, (4) can be rewritten in the state–space form

$$\dot{z}(t) = Az(t) + B_1u(t) + B_2f(t) \tag{5}$$

where $z = [x^T\ \dot{x}^T]^T$, $A = \begin{bmatrix} \mathbf{0}_{m\times m} & I_{m\times m} \\ \mathbf{0}_{m\times m} & -M_d^{-1}C_d \end{bmatrix}$ and $B_1 = B_2 = \begin{bmatrix} \mathbf{0}_{m\times m} \\ M_d^{-1} \end{bmatrix}$, with $\mathbf{0}_{m\times m}$ and $I_{m\times m}$ denoting $m \times m$ zero and unit matrices, respectively. To solve the optimal tracking problem, it needs to be transformed to a regulation problem [28]. In particular, the desired trajectory x_d is generated by a given system

$$\begin{cases} \dot{w} = Uw \\ x_d = Vw \end{cases} \tag{6}$$

where $w \in \mathbb{R}^l$ is an auxiliary state, and $U \in \mathbb{R}^{l\times l}$ and $V \in \mathbb{R}^{n\times l}$ are two matrices designed to generate x_d. Then, by denoting $\bar{z} = [z^T\ w^T]^T$, we have the augmented system

$$\dot{\bar{z}} = \bar{A}\bar{z} + \bar{B}_1u + \bar{B}_2f \tag{7}$$

where $\bar{A} = \begin{bmatrix} A & \mathbf{0}_{2m\times l} \\ \mathbf{0}_{l\times 2m} & U \end{bmatrix}$, $\bar{B}_1 = \bar{B}_2 = \begin{bmatrix} B_1 \\ \mathbf{0}_{l\times m} \end{bmatrix}$, and $\mathbf{0}_{2m\times l}$, $\mathbf{0}_{l\times 2m}$, and $\mathbf{0}_{l\times m}$ denote zero matrices with proper dimensions.

B. Problem Formulation

We consider that the robot's control objective is to minimize the infinite-horizon cost function

$$\begin{aligned} \Gamma &= \int_0^\infty c(t)dt \\ c(t) &= (x - x_d)^T Q_1 (x - x_d) + \dot{x}^T Q_2 \dot{x} + u^T R_1 u \\ &\quad + f^T R_2 f \end{aligned} \tag{8}$$

where $Q_1, Q_2 \in \mathbb{R}^{m\times m} \succeq 0$ and $R_1, R_2 \in \mathbb{R}^{m\times m} \succ 0$ are the weights. The first term of the above cost function penalizes the error between the actual and desired positions of the robot, while the second term regulates the velocity. The last two terms determine the contributions of the human and the robot: a higher R_1 indicates a higher propensity for the human to lead, and conversely, a higher R_2 indicates a higher propensity for the robot to lead.

Remark 1: In [10], the desired trajectory is solely determined by the human, and the strategy of the robot is to track the intended motion of the human. In comparison with [10], the cost function defined by (8) describes a more general situation, where the desired trajectory is determined/negotiated by both the human and the robot. The situation discussed in [10] is thus a special case, either when the weight R_1 is chosen to be very large, or when the desired trajectory of the robot x_d is identical to the intention of the human. Conversely, if the weight R_1 is chosen to be relatively small, the decision of the robot will be more respected. This is especially useful in situations when the robot should take the lead, e.g., precise positioning as discussed in Section I.

According to the definition of the augmented state $\bar{z}$, the cost function (8) can be rewritten as

$$\Gamma = \int_0^\infty (\bar{z}^T Q \bar{z} + u^T R_1 u + f^T R_2 f)dt \tag{9}$$

where $Q = \begin{bmatrix} Q_1 & \mathbf{0}_{m\times m} & -Q_1 V \\ \mathbf{0}_{m\times m} & Q_2 & \mathbf{0}_{m\times l} \\ -V^T Q_1 & \mathbf{0}_{l\times m} & V^T Q_1 V \end{bmatrix}$. In human–robot shared control, the robot should change its control objective according to the human's. Therefore, we expect that the human's objective can be also described by minimization of a cost function.

Assumption 1: The cost function structure of the human is the same as that of the robot, which is described in (9).

However, the human's cost function is typically unknown to the robot. Therefore, in the remainder of this paper, we aim to develop a method to adapt the robot's cost function based on interactions with the human.

C. Game Theory

Human–robot shared control can be studied based on game theory. In particular, the human and the robot are involved in a common game and have individual objectives (described by individual cost functions). In game theory, different types of multiagent behaviors, such as cooperation and competition, have been defined and analyzed [26]. We follow the characterization of multiagent behaviors in terms of the relationship between the cost functions of individual agents [29], [30]. There are different solution concepts to the game that will result in different multiagent behaviors, and Nash equilibrium is considered in this paper.

Definition 2: Coordination refers to the case that the cost functions of all agents are the same.

Based on Assumption 1 and Definition 2, coordination is realized in human–robot shared control if the human's cost function is also Γ. Then, the Nash equilibrium can be achieved by the optimal control

$$u^* = -\frac{1}{2} R_1^{-1} \bar{B}_1^T P \bar{z}^* \tag{10}$$

$$f^* = -\frac{1}{2} R_2^{-1} \bar{B}_2^T P \bar{z}^* \tag{11}$$

where P is obtained by solving the following well-known Riccati equation [31]

$$\begin{aligned} &\bar{A}^T P + P\bar{A} + Q - P\bar{B}_1 R_1^{-1} \bar{B}_1^T P \\ &\quad - P\bar{B}_2 R_2^{-1} \bar{B}_2^T P = \mathbf{0}_{m\times m} \end{aligned} \tag{12}$$

and $\bar{z}^*$ denotes the optimal state in the following optimal system:

$$\dot{\bar{z}}^* = \bar{A}\bar{z}^* + \bar{B}_1 u^* + \bar{B}_2 f^*. \tag{13}$$

Remark 2: Note that the Riccati (12) takes into account the interaction between two agents (the human and the robot) and their shared control of the same system. It is different from the linear quadratic regulator for an individual agent, given by

$$\bar{A}^T P + P\bar{A} + Q - P\bar{B}_1 R_1^{-1} \bar{B}_1^T P = \mathbf{0}_{m\times m} \tag{14}$$

for the cost function $\int_0^\infty [\bar{z}^T Q \bar{z} + u^T R_1 u]dt$, and by

$$\bar{A}^T P + P\bar{A} + Q - P\bar{B}_2 R_2^{-1} \bar{B}_2^T P = \mathbf{0}_{m\times m} \tag{15}$$

for the cost function $\int_0^\infty [\bar{z}^T Q \bar{z} + f^T R_2 f]dt$. x

As discussed in the previous section, the cost function of the human is unknown to the robot and probably not equal to Γ. This leads to different Nash equilibria, which require control inputs different from (10) and (11). As the actual control input of the human f is measurable, the difference between f and f^* in (11) can be used as a measure of conflict between the human's objective and that of the robot, i.e., eliminating the difference will realize the coordination of the human and the robot. Based on this idea, we will develop a role adaption method, which is detailed in the following section.

III. Role Adaptation for Human–Robot Coordination

The relative roles of the human and the robot can be adapted by updating either R_1 or R_2 in the cost function (8) to minimize $E = \frac{1}{2} e_f^T e_f$, where $e_f = f - f^*$. We realize this with the adaptation law

$$\dot{R}_2 = -\alpha \frac{\partial E}{\partial R_2} \tag{16}$$

where $\alpha > 0$ is the update rate.

Whenever the human interacts with the robot by exerting a force f, the weight R_2 will be updated via (16) until f tracks the optimal control f^* with a new cost function and a new R_2. In other words, the human claims a new role by applying a force f, which will result in a force error, and the robot will adapt to this new role by reducing the force error. This can be intuitively understood through two illustrative cases. In the first case, suppose that the human does not want to lead; he/she would reduce the interaction force applied to the robot. Then, the adaptation law increases R_2 to the effect of increasing the penalty of the human input in the cost function. As a result, u increases to make the robot take on a greater leading role. In the second case, if the human wants to lead the task, he/she would apply a larger force to the robot. This causes the adaptation law to decrease R_2 to the effect of increasing the penalty of the robot input in the cost function, thereby causing the robot to give up a portion of the shared control.

For ease of implementation, we let $R_2 = r_2 I_{m\times m}$. This simplifies the adaptation law to

$$\dot{r}_2 = -\alpha \frac{\partial E}{\partial r_2} = -\alpha e_f^T \frac{\partial e_f}{\partial r_2}. \tag{17}$$

According to (11), we have

$$\frac{\partial e_f}{\partial r_2} = \frac{1}{2r_2^2}\bar{B}_2^T P\bar{z}^* - \frac{1}{2r_2}\bar{B}_2^T \frac{\partial P}{\partial r_2}\bar{z}^* - \frac{1}{2r_2}\bar{B}_2^T P\frac{\partial \bar{z}^*}{\partial r_2} \tag{18}$$

where $P(t)$ is obtained by solving (12). $\frac{\partial P}{\partial r_2}$ is obtained by solving

$$\begin{aligned}\bar{A}^T\frac{\partial P}{\partial r_2} + \frac{\partial P}{\partial r_2}\bar{A} - \frac{\partial P}{\partial r_2}\bar{B}_1 R_1^{-1}\bar{B}_1^T P \\ - P\bar{B}_1 R_1^{-1}\bar{B}_1^T\frac{\partial P}{\partial r_2} - \frac{\partial P}{\partial r_2}\bar{B}_2 R_2^{-1}\bar{B}_2^T P \\ - P\bar{B}_2 R_2^{-1}\bar{B}_2^T\frac{\partial P}{\partial r_2} + \frac{1}{r_2^2}P\bar{B}_2\bar{B}_2^T P = \mathbf{0}_{m\times m}\end{aligned} \tag{19}$$

which is obtained by differentiating (12) with respect to r_2. By denoting

$$\begin{aligned}X &= \bar{A} - (\bar{B}_1 R_1^{-1}\bar{B}_1^T + \bar{B}_2 R_2^{-1}\bar{B}_2^T)P \\ Y &= -\frac{1}{r_2^2}P\bar{B}_2\bar{B}_2^T P.\end{aligned} \tag{20}$$

We can rewrite (19) as

$$X^T\frac{\partial P}{\partial r_2} + \frac{\partial P}{\partial r_2}X = Y. \tag{21}$$

Then, we have

$$\frac{\partial P}{\partial r_2} = \frac{1}{2}X^{-T}Y \tag{22}$$

by considering that $\frac{\partial P}{\partial r_2}$ and Y are symmetric. In addition, from (13), we can obtain

$$\dot{\bar{z}}^* = \dot{r}_2\frac{\partial \bar{z}^*}{\partial r_2}. \tag{23}$$

Finally, by substituting (17) and (18) into (23), we obtain $\frac{\partial \bar{z}^*}{\partial r_2}$, and thus $\frac{\partial e_f}{\partial r_2}$ in (18).

Algorithm 1: Role adaptation

Input: The current state $\bar{z}$ and the measured interaction force f.

Output: The reference velocity in the joint space $\dot{q}_r$.

begin

Set M_d and C_d in the impedance model (4). Set U and V in (6) to generate x_d. Initialize $\bar{z}^* = \bar{z}$ and the weights Q_1, Q_2, R_1, and R_2 in the cost function (8). Set parameter α in the adaptation law (17).

while $t < t_f$ *where* t_f *is the terminal time* **do**

Collect the current state $\bar{z} = [x^T\ \dot{x}^T\ w^T]^T$ and the measured interaction force f.
Calculate P by solving (12).
Calculate optimal controls u^* and f^* in (10) and (11), respectively.
Obtain the optimal state $\bar{z}^*$ in (13).
Obtain the control input of the robot u in (24).
Calculate the reference velocity $\dot{x}_r$ in (2).
Obtain the reference velocity in the joint space $\dot{q}_r$ according to (3).
Update R_2 according to (17), (18), (22), and (23).

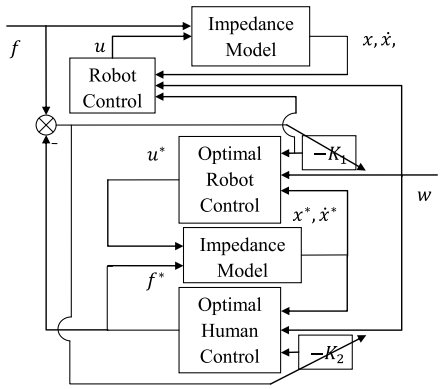

Fig. 2. Proposed control framework.

After R_2 is updated and P obtained, the actual control input of the robot can be designed as

$$u = -\frac{1}{2}R_1^{-1}\bar{B}_1^T P\bar{z}. \tag{24}$$

Implementation procedures of the proposed role adaptation method are summarized in Algorithm 1.

The block diagram of the proposed control framework is given in Fig. 2 , where $K_1 = \frac{1}{2}R_1^{-1}\bar{B}_1^T P$ and $K_2 = \frac{1}{2}R_2^{-1}\bar{B}_2^T P$ are the optimal feedback gains for the robot and the human, respectively. Since P is updated during role adaptation, the gain K_1 will also be changed. To understand the effect of role adaptation on the impedance, we first write the impedance model (4) in the form

$$M_d\ddot{x}(t) + C_d\dot{x}(t) + K_1\bar{z} = f. \tag{25}$$

Substituting $K_1 = [K_{1,1}K_{1,2}K_{1,3}]$, where $K_{1,1} \in \mathbb{R}^{m\times m}$, $K_{1,2} \in \mathbb{R}^{m\times m}$, and $K_{1,3} \in \mathbb{R}^{m\times l}$, we obtain

$$M_d\ddot{x}(t) + (C_d + K_{1,1})\dot{x}(t) + (K_{1,2}x + K_{1,3}w) = f. \tag{26}$$

which clearly shows that stiffness is modulated by $K_{1,2}$ and $K_{1,3}$, and damping by $K_{1,1}$. Note that the stiffness component $(K_{1,2}x + K_{1,3}w)$ includes the desired trajectory of the robot x_d [recalling (6)]. As such, the resulting control u can be viewed as a variable impedance control where the damping and stiffness parameters are concurrently adapted [32]. Through experimental studies in the next section, we will show that this control makes the robot more compliant when the human is leading the task, but stiffer when the robot is leading.

Theorem 1: Consider the robot dynamics governed by the given impedance model (4). If f is of class C^2, the control input (24) with the developed role adaptation law (17) will guarantee that

1) $\lim_{t\to\infty} e_f(t) = 0$, which indicates that the human control input is optimal in the sense of minimizing the cost function (8);
2) $\lim_{t\to\infty} u(t) = u^*(t)$, which indicates that the robot control input is optimal; and
3) all the other closed-loop signals are bounded.

Proof: By subtracting (13) from (7), we have

$$\dot{e}_{\bar{z}} = \bar{A}e_{\bar{z}} + \bar{B}_1(u - u^*) + \bar{B}_2 e_f \tag{27}$$

where $e_{\bar{z}} = \bar{z} - \bar{z}^*$. By considering optimal control (10) and actual control (24), we have

$$\dot{e}_{\bar{z}} = (\bar{A} - \bar{B}_1 K_1)e_{\bar{z}} + \bar{B}_2 e_f. \tag{28}$$

Consider the following Lyapunov function candidate

$$W = E + \frac{\chi}{2} e_{\bar{z}}^T e_{\bar{z}} \tag{29}$$

where $\chi = \frac{4\alpha\lambda_1\lambda_2}{\|\bar{B}_2\|^2}$, with λ_1 being the lower bound of the minimum eigenvalue of $\frac{\partial e_f}{\partial r_2}(\frac{\partial e_f}{\partial r_2})^T$ and λ_2 the minimum eigenvalue of $\bar{B}_1 K_1 - \bar{A}$.

By differentiating (29) with respect to time, and considering (17) and (28), we obtain

$$\begin{aligned}
\dot{W} =& \left(\frac{\partial E}{\partial r_2}\right)^T \dot{r}_2 + \chi e_{\bar{z}}^T \dot{e}_{\bar{z}} \\
=& -\alpha e_f^T \frac{\partial e_f}{\partial r_2}\left(\frac{\partial e_f}{\partial r_2}\right)^T e_f + \chi e_{\bar{z}}^T(\bar{A} - \bar{B}_1 K_1)e_{\bar{z}} \\
&+ \chi e_{\bar{z}}^T \bar{B}_2 e_f \\
\le& -\alpha\lambda_1\|e_f\|^2 - \chi\lambda_2\|e_{\bar{z}}\|^2 + \chi e_{\bar{z}}^T \bar{B}_2 e_f \\
=& -(\sqrt{\alpha\lambda_1}\|e_f\| - \sqrt{\chi\lambda_2}\|e_{\bar{z}}\|)^2 \\
&-2\sqrt{\alpha\chi\lambda_1\lambda_2}\|e_f\|\|e_{\bar{z}}\| + \chi e_{\bar{z}}^T \bar{B}_2 e_f \\
\le& (-2\sqrt{\alpha\chi\lambda_1\lambda_2} + \chi\|\bar{B}_2\|)\|e_f\|\|e_{\bar{z}}\| = 0.
\end{aligned} \tag{30}$$

According to (30), if $\lambda_1 \neq 0$, e_f and $e_{\bar{z}}$ are bounded; otherwise, (17) indicates $\dot{r}_2 = 0$, and thus, e_f and $e_{\bar{z}}$ are bounded. According to (28), $\dot{e}_{\bar{z}}$ is also bounded.

According to Barbalat's lemma [33], we need to verify the boundedness of $\ddot{W}$ to conclude the asymptotic stability of the system under study. Therefore, we differentiate (30) and obtain

$$\ddot{W} = e_f^T \ddot{e}_f + \dot{e}_f^T \dot{e}_f + \chi e_{\bar{z}}^T \ddot{e}_{\bar{z}} + \chi \dot{e}_{\bar{z}}^T \dot{e}_{\bar{z}}. \tag{31}$$

From (31), we know that if $\dot{e}_f$, $\ddot{e}_f$, and $\ddot{e}_{\bar{z}}$ are bounded, then $\ddot{W}$ is bounded.

Since f is exerted by the human and it is bounded, f^* is bounded. By comparing (11) and (10), and considering (12), we obtain that u^* is bounded, as well as P and $\dot{P}$. Hence, $\dot{r}_2$ is bounded according to (17), and $\bar{z}^*$ and $\dot{\bar{z}}^*$ are bounded according to (13). By considering (11), we have

$$\dot{e}_f = \dot{f} - \frac{\dot{r}_2}{2r_2}\bar{B}_2^T P\bar{z}^* + \frac{1}{2r_2}\bar{B}_2^T \dot{P}\bar{z}^* + \frac{1}{2r_2}\bar{B}_2^T P\dot{\bar{z}}^*. \tag{32}$$

Since $\dot{f}$ is bounded, $\dot{e}_f$ is bounded. By differentiating (32), we have

$$\begin{aligned}
\ddot{e}_f =& \ddot{f} - \frac{\ddot{r}_2}{2r_2^2}\bar{B}_2^T P\bar{z}^* - \frac{\dot{r}_2}{2r_2^2}\bar{B}_2^T \dot{P}\bar{z}^* - \frac{\dot{r}_2}{2r_2^2}\bar{B}_2^T P\dot{\bar{z}}^* \\
&+ \frac{1}{2r_2}\bar{B}_2^T \ddot{P}\bar{z}^* + \frac{1}{r_2}\bar{B}_2^T \dot{P}\dot{\bar{z}}^* + \frac{1}{2r_2}\bar{B}_2^T P\ddot{\bar{z}}^*.
\end{aligned} \tag{33}$$

In (33), we have that $\ddot{r}_2$ is bounded by differentiating (17), and $\ddot{P}$ is bounded by differentiating (12). By considering (10), we know that $\dot{u}^*$ is bounded. By differentiating (13), we have that $\ddot{\bar{z}}^*$ is bounded. Hence, $\ddot{e}_f$ is bounded. Besides, we have that $\ddot{e}_{\bar{z}}$ is bounded by differentiating (28).

Therefore, we can conclude that $\ddot{W}$ is bounded. According to Barbalat's lemma [33], we can claim that $\lim_{t\to\infty} e_f(t) = 0$ and $\lim_{t\to\infty} e_{\bar{z}}(t) = 0$, which lead to $\lim_{t\to\infty} u(t) = u^*(t)$, by considering (24). This completes the proof. ■

Remark 3: Following Theorem 1, we elaborate how to design control (24) given design requirements such as the bound of the input signal. By substituting control (24) to the augmented system (7), we have the closed-loop system described by $\dot{\bar{z}} = (\bar{A} - \bar{B}_1 K_1)\bar{z} + \bar{B}_2 f$, which has the solution $\bar{z}(t) = e^{(\bar{A}-\bar{B}_1 K_1)t}\bar{z}(0) + \bar{B}_2 \int_0^t f(s)ds$. The two terms in this solution are two parts of the system state: the first under the robot control and the second under the human control. Because the second part is determined by the human, we have to assume that the human does not cause the system instability on purpose, i.e., $\|\int_0^t f(s)ds\| \le b_f$ where b_f is a positive scalar. Because the eigenvalues of $\bar{A} - \bar{B}_1 K_1$ are negative, we have $\|\bar{z}(t)\| \le \|\bar{z}(0)\| + b_f\|\bar{B}_2\|$. Considering (24) and this inequality, we obtain

$$\begin{aligned}
\|u\| =& \frac{\|\bar{B}_1\|\|P\|}{2\|R_1\|}\|\bar{z}\| \\
\le& \frac{\|\bar{B}_1\|\|P\|}{2\|R_1\|}(\|\bar{z}(0)\| + b_f\|\bar{B}_2\|).
\end{aligned} \tag{34}$$

According to the above inequality, the bound of u is determined by values of the following parameters: $\bar{B}_1$, P, R_1, and $\bar{B}_2$. Suppose that rough knowledge of b_f is available, M_d and C_d in the impedance model (4), which relate to $\bar{A}$, $\bar{B}_1$, and $\bar{B}_2$, are chosen by considering $b_f\|\bar{B}_2\|$. Then, the weights Q_1, Q_2, and R_1 in cost function (8), which relate to P, are chosen by considering $\frac{\|\bar{B}_1\|\|P\|}{2\|R_1\|}$.

IV. Experiments

In the following, the units of all variables are SI units, unless otherwise stated.

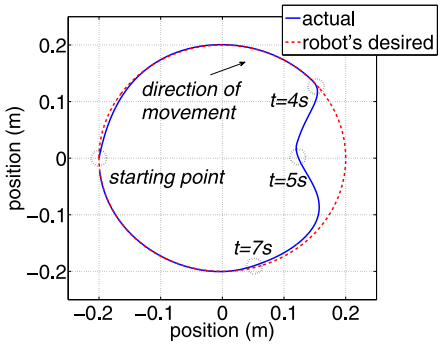

Fig. 3. Trajectory of the robot.

A. Experiment I: Adaptation to Different Force Levels

In this experiment, we considered a scenario where a robot with two revolute joints moved in a planar space and an external force was applied to its end-effector by a human.

1) Settings: As discussed in Section II, the dynamics of the robot were governed by an impedance model (4), where $M_d = I_{2\times 2}$ and $C_d = I_{2\times 2}$. The desired trajectory of the robot was a circle with a radius of 0.2 m, i.e., $x_d = [-0.2\cos(\frac{\pi}{5}t), 0.2\sin(\frac{\pi}{5}t)]^T$. It was generated by (6) with $U = \begin{bmatrix} 0 & \frac{\pi}{5} \\ -\frac{\pi}{5} & 0 \end{bmatrix}$ and $V = \frac{1}{\pi}I_{2\times 2}$. The initial weights in the cost function (8) were set as $Q_1 = 50I_{2\times 2}$, $Q_2 = I_{2\times 2}$, $R_1 = 0.5I_{2\times 2}$, and $R_2 = 20I_{2\times 2}$. The rationale for choosing these initial values is: if there is no human intervention, the robot should lead the task (with a small R_1 and a large R_2) and the control objective is to track the desired trajectory (with a large Q_1). The update rate in the adaptation law (16) was $\alpha = 5000$. If r_2 becomes too small (large), the human (the robot) may take full control of the system. It is dangerous for an inexperienced human to take full control of the system, while it is very difficult to interact with a robot under its own full control. Therefore, to prevent r_2 from becoming too small, we set a lower bound, i.e., the value of r_2 was set as 0.4 if it was smaller than 0.4. To clearly show the results of role adaptation, we considered different force levels applied by the human at different time intervals, i.e.,

$$f_X = \begin{cases} 0\text{ N}, & t \le 4\text{ s} \\ 0.5\text{ N}, & 4\text{ s} < t \le 5\text{ s} \\ 0.1\text{ N}, & 5\text{ s} < t \le 7\text{ s} \\ 0\text{ N}, & t > 7\text{ s} \end{cases}$$

and $f_Y = 0$N for $t \in [0, 10]$s, where the subscripts $_X$ and $_Y$ represent the respective directions.

2) Results: The result of the trajectory tracking is shown in Fig. 3. When the interaction force was applied by the human from 4 s to 7 s, the actual trajectory of the robot deviated from the desired trajectory; otherwise, the actual trajectory of the robot tracked the desired one.

Results of the role adaptation are shown in Figs. 4 and 5, where the whole process is divided into four stages.

In the first stage, the weight r_2 converged to a certain value when there was no interaction force and the robot was leading the task to track the desired trajectory.

In the second stage, the human applied a force of 0.5 N to the robot; therefore, r_2 decreased to reduce the penalty of the human input in the cost function. As a result, the feedback gain of the robot K_1 decreased in this stage, indicating that the robot became more compliant to give up a higher portion of shared control to the human. Conversely, the optimal feedback gain of the human K_2 increased. The crossover of the two feedback gains in the second stage clearly shows the exchange of roles between the human and the robot. Fig. 5 illustrates that role adaptation decreased the error between the optimal force f^* and the actual force f.

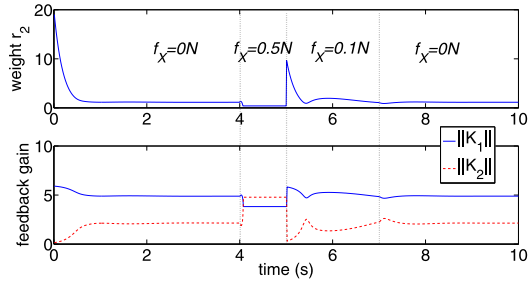

Fig. 4. Weight of the interaction force (top), and feedback gains of the robot and the human (bottom).

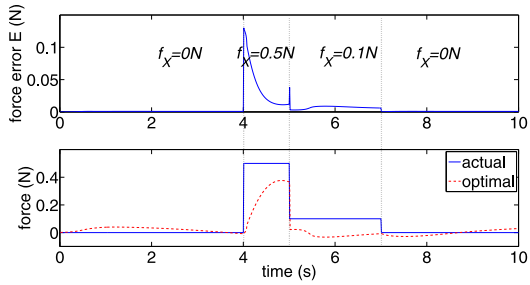

Fig. 5. Force error (top) and the interaction force (bottom).

In the third stage, because a relatively smaller force was applied to the robot (0.1N), a portion of the control shifted from human to robot. Therefore, r_2 became larger than in the second stage, as did K_1, to make the robot stiffer. Nonetheless, the error between the optimal force f^* and actual force f became smaller, as shown in Fig. 5.

In the fourth stage, the interaction force was set to zero, and r_2 converged back to the same value in the first stage. Note that there are large overshoots in Figs. 4 and 5. This is because the interaction force was switched from a constant to another. In a real-world scenario, the human would change force in a smoother way; therefore, the large overshoots should not exist.

From the previously mentioned results, we conclude that the following expected behavior of the robot was achieved: When the human intervened to lead a task by applying a larger force, the robot became more compliant; when the human was satisfied with the current situation and did not intervene, the robot tried to lead the task. Thus, the role adaptation was triggered from the human side and was achieved automatically by the robot.

B. Experiment II: User Study

As uncertainties of the human behavior and human motor control cannot be described in above simulations, we further verify the validity of the proposed method through a user study.

1) Settings: The experiment setup is illustrated in Fig. 6, where a 7-DOF Meka A1 arm was used as the experiment

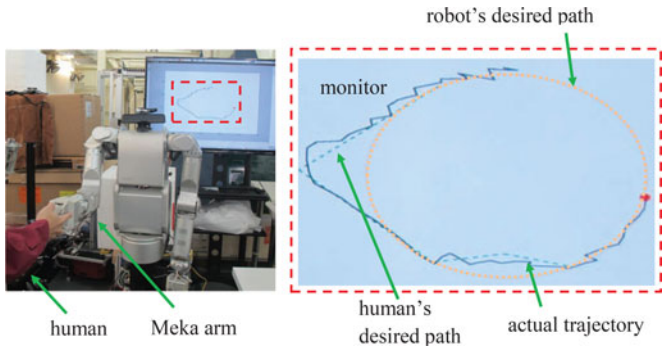

Fig. 6. Experiment setup.

platform. Each of its joint was under position control and its reference velocity $\dot{q}_r$ was obtained from Algorithm 1. The joint angle was measured directly by the ContElec Vert-X 13 encoder at the joint, and the velocity was filtered by a low-pass filter with cutoff frequency of 20 Hz. A 6-axis ATI load cell was used for direct sensing of the tool force/torque wrench, and it was attached to the tool plate of the arm. There was a 40-in monitor behind the Meka robot to display the human's and the robot's desired paths, and the actual trajectory of the robot end-effector.

The desired path of the robot end-effector was a circle on a vertical plane in front of the robot, parallel to its frontal plane. The desired trajectory was $x_d = [0.125\cos(t), 0.125\sin(t)]$. The human's desired path was different, comprising an arc overlapping with the aforementioned circle and four straight line segments. These path segments were joined at the points: $x_{h,1} = [-0.063, 0.104]^T$, $x_{h,2} = [-0.185, 0]^T$, $x_{h,3} = [-0.063, -0.104]^T$, $x_{h,4} = [0, -0.095]^T$, and $x_{h,5} = [0.063, -0.104]^T$. Based on the human's desired path, we defined the tracking error as

$$e = \begin{cases} x - x_d, & t_0 < t \le t_1 \\ x - x_{h,1} - \dfrac{(x_{h,2} - x_{h,1})}{t_2 - t_1}(t - t_1), & t_1 < t \le t_2 \\ x - x_{h,2} - \dfrac{(x_{h,3} - x_{h,2})}{t_3 - t_2}(t - t_2), & t_2 < t \le t_3 \\ x - x_{h,3} - \dfrac{(x_{h,4} - x_{h,3})}{t_4 - t_3}(t - t_3), & t_3 < t \le t_4 \\ x - x_{h,4} - \dfrac{(x_{h,5} - x_{h,4})}{t_5 - t_4}(t - t_4), & t_4 < t \le t_5 \\ x - x_d, & t_5 < t \le t_6. \end{cases}$$

where $t_0 = 0.0$ s, $t_1 = 3.6$ s, $t_2 = 8.8$ s, $t_3 = 14.0$ s, $t_4 = 16.8$ s, $t_5 = 19.6$ s, and $t_6 = 32.0$ s. This setting was motivated by the application of robotic welding: while the robot was automated to follow a prescribed trajectory with a basic shape (a circle in this setting), the human might have some position points of interest based on the actual odd shape of a workpiece ($x_{h,2}$ and $x_{h,4}$ in this setting). We selected the impedance parameters as $M_d = 5I_{2\times2}$ and $C_d = 750I_{2\times2}$, the initial weights as $Q_1 = 10^5 I_{2\times2}$, $Q_2 = I_{2\times2}$, and $R_1 = 0.001I_{2\times2}$, and the adaptation rate as $\alpha = 10$. To show the significance of the proposed method, the following conditions were compared: "robot leading" with $r_2 \equiv 0.01$, "human leading" with $r_2 \equiv 0.0001$, and "adaptation" with $r_2(0) = 0.01$. To prevent r_2 from becoming too small or too large, we set lower and upper bounds as follows: if the value of r_2 was smaller than 0.0001, it was set as 0.0001; and if the value of r_2 was larger than 0.01, it was set as 0.01.

Ten subjects participated in the experiment. They were informed that there were three different experimental conditions, but were not told what they were. For each condition, the subject was instructed to stand in front of the robot facing the monitor, and move the end-effector along the human's desired path shown on the monitor. Subjects were allowed to practise until they were familiar with the task. Subsequently, each subject performed five trials of each experimental condition.

2) Results: For clarity and conciseness, we only show results from representative trials in Figs. 7 and 8. It is clear from Fig. 7 that the actual end-effector path under the "adaptation" condition was close to the human's desired path. On the other hand, the end-effector fell short of reaching the leftmost point on the human's desired path under the "robot leading" condition, while the tracking error was smaller along the curved segment where both desired paths overlap. Besides this, the force vectors illustrate that larger forces were needed for the "robot leading" condition when the desired paths were different. These experimental results are largely in line with expectations, except for the tracking performance under the "human leading" condition, in which the end-effector did not follow the human's desired path closely even though it should. This is likely to be due to the underdamped human motion resulting in frequent overshooting when moving the robot in the "human leading" condition. Note that the above comparisons are not valid point by point due to the variance of the human dynamics across trials. Therefore, we will perform statistical analysis in the following to study the effect of the proposed method. In Fig. 8, we show the weight of the human contribution to the shared control, r_2^{-1}, the robot control gain K_1, as well as the profiles of the tracking error and the interaction force. The results show that increased interaction force led to an increase of the weight r_2^{-1} but a decrease of the gain K_1 that makes it easy for the human to take the lead. The converse is also true, i.e., decreased interaction force is accompanied by a decrease of r_2^{-1} but an increase of K_1, allowing the robot to regain control.

For analysis purpose, the human's desired path was divided into two segments. The first segment consists of the straight line segments that were not found in the robot's desired path. The second segment comprises the circular arc that overlapped with the robot's desired path. Then, for each segment as well as the complete path, we carry out quantitative evaluation of the outcome from the different experimental conditions based on the following measures:

1) *First Segment:* tracking error $\mathcal{E}_1 = \int_{t_1}^{t_5} \|e(t)\|dt$ and interaction force $\mathcal{F}_1 = \int_{t_1}^{t_5} \|f(t)\|dt$
2) *Second Segment:* tracking error $\mathcal{E}_2 = \int_{t_0}^{t_1} \|e(t)\|dt + \int_{t_5}^{t_6} \|e(t)\|dt$ and interaction force $\mathcal{F}_2 = \int_{t_0}^{t_1} \|f(t)\|dt + \int_{t_5}^{t_6} \|f(t)\|dt$
3) *Complete Path:* tracking error $\mathcal{E} = \int_{t_0}^{t_6} \|e(t)\|dt$, interaction force $\mathcal{F} = \int_{t_0}^{t_6} \|f(t)\|dt$, and work done $\mathcal{W} = \int_{t_0}^{t_6} \|f^T(t)\dot{x}(t)\|dt$

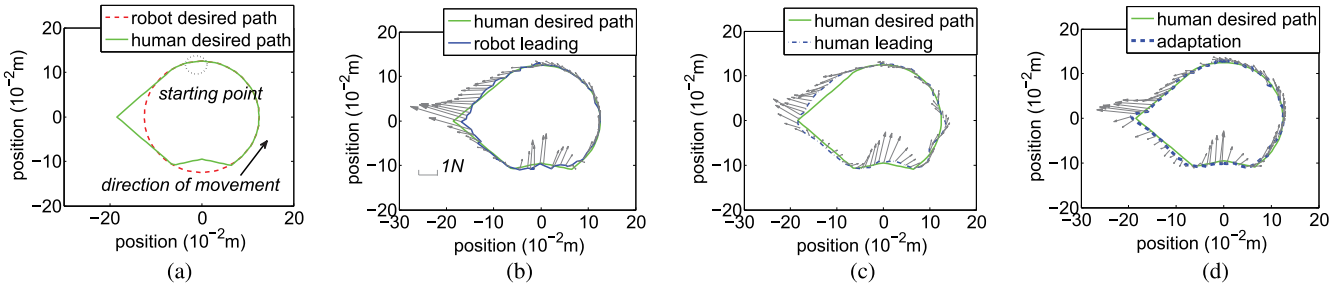

Fig. 7. Trajectories of Meka's end-effector for adaptive- and fixed-role cases. Each gray arrow shows the force vector at the corresponding position point along the trajectory.

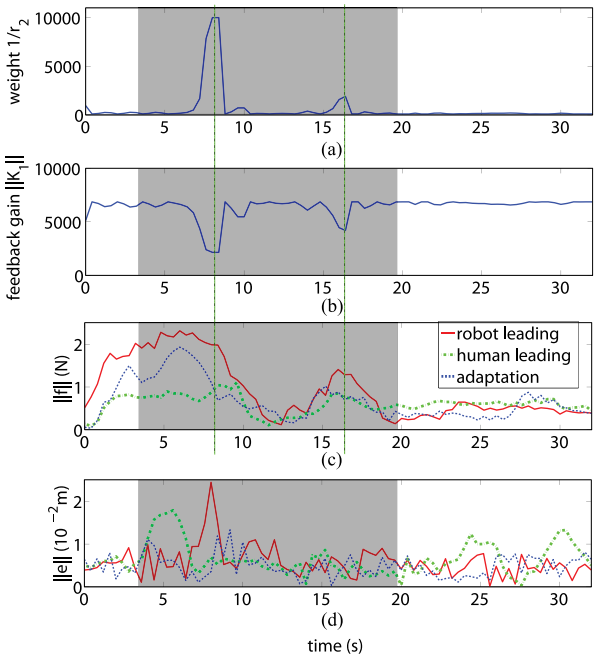

Fig. 8. (a) Weight of the interaction force, (b) robot control gain, (c) tracking error, and (d) interaction force. The shadow in each subplot indicates the segment when the robot's and the human's desired paths are different. The two large peaks/troughs at $t = 8$ s and $t = 17$ s in (a), (b), and (c) indicate the time when the subject wanted to lead. The small peaks/troughs at $t = 10$ s in (a) and (b) are due to the overshoot during the adaptation process.

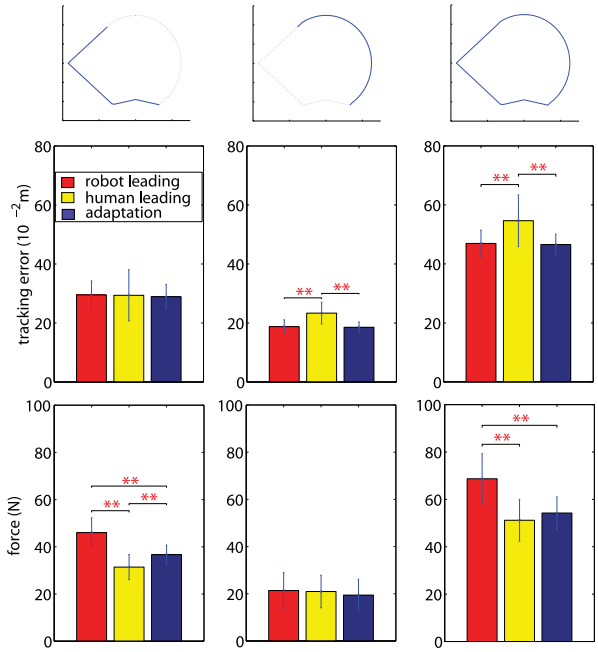

Fig. 9. Comparison of performance measures: the tracking error and the interaction force along the first segment, the second segment, and the complete path (indicated by the solid lines in the three top diagrams). A double asterisk "**" indicates $p < 0.001$.

Then, we employed one-way analysis of variance (ANOVA) to test the null hypothesis that there is no difference between the population means for the three experimental conditions. The mean and standard deviation of the above measures were computed using 50 data points for each experimental condition (5 trials $\times$ 10 users).

The first column ofFig. 9 is for the first segment and shows that the null hypothesis was rejected for the interaction force but not the tracking error. In particular, the interaction force for the "adaptation" and "human leading" conditions were significantly smaller ($p < 0.001$) than that for the "robot leading" condition.

The second column of Fig. 9 corresponds to the second segment and shows that the null hypothesis was rejected for the tracking error but not the interaction force. It is observed that the tracking error for the "adaptation" condition is significantly smaller ($p < 0.001$) than that for the "human leading" condition. That the interaction forces were similar across the conditions is due to the overlap in the desired paths, which obviated the need for corrective intervention from the subjects.

For measures involving the complete path, as shown in the third column of Fig. 9, the null hypothesis was rejected for both tracking error and interaction force. The tracking errors for the "adaptation" and "robot leading" conditions were significantly smaller ($p < 0.001$) than that for the "human leading" condition, while the interaction forces for the "adaptation" and "human leading" conditions were significantly smaller ($p < 0.001$) than that for the "robot leading" condition. Besides this, the work done $\mathcal{W}$ for the "adaptation" and "human leading" conditions was significantly smaller ($p < 0.01$ and $p < 0.001$, respectively) than that for the "robot leading" condition, as shown in Fig. 10.

The above results demonstrate that role adaptation achieved the best overall performance, in the sense of minimizing both human effort and trajectory tracking error, as compared with fixed-role strategies (human or robot leading) that were limited by a tradeoff between effort and error.

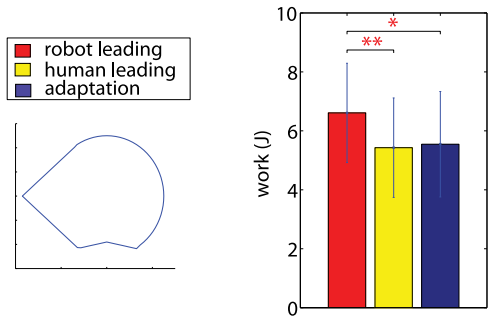

Fig. 10. Comparison of performance measures: the work done by subjects along the complete path (indicated by the solid line in the left diagram). A single asterisk "*" indicates $p < 0.01$, and a double asterisk "**" indicates $p < 0.001$.

V. Discussions

As discussed in Section I, role adaptation should take place when the current performance is unsatisfactory. The proposed method only considers the situation when the human is unsatisfied, i.e., the role adaptation is engaged by the human changing the interaction force applied to the robot. The situation when the robot engages the adaptation is task-dependent. For example, in robotic painting, the robot can be assigned a leading role when it is in close proximity to the painting surface. We do not have a generic framework to handle this situation, other than giving the robot a higher level authority.

Although not revealed by the experimental results, the issue of coadaptation exists and should be further addressed. When the proposed method adapts the robot's motion to the human's, the human may also adapt his/her motion intention according to the robot's motion. As a result, adverse effects such as oscillation and even instability may take place. The future works may be focused on looking for convergence conditions of coadaptation.

As discussed in Section III, the proposed method results in a variable impedance control with the robot's impedance parameters adapted to the human's different intentions. However, the robot's reference trajectory should also be adapted, otherwise, there will be additional interaction force and even wind-up due to the possible difference between the robot's actual velocity and the human's desired one. Therefore, to realize the reference adaptation in the proposed framework is also one of our future works.

During the experiments, we find that the update rate α in (16) should be carefully selected: if adaptation is too slow, it is unable to guarantee a good performance, but if adaptation is too fast, it may create discomfort for the user and lead to a worse performance. The current trial-and-error procedure is time-consuming and impractical. This problem leads to a fundamental issue that we have not addressed in this study: where, explicitly, are the Nash equilibria during adaptation, and how to determine if they even exist? In particular, we have only shown that the proposed method achieves a better performance by implicitly adjusting the robot's role in a two-agent game. These open problems will be investigated in our future works.

VI. Conclusion

Human–robot shared control has been studied based on game theory in this paper. A continuous adaptation law has been developed to make the robot change its role according to the interaction force applied by the human, such that coordination is achieved. The adaptation behaviors with different force levels has been observed through an experimental study. Moreover, the proposed method has been compared with fixed-role interactions through a user study, which has demonstrated that the former yields better overall performance than the later. Limitations of the proposed method and possible future works have been also discussed.

References

[1] R. Riener, A. Duschau-Wicke, A. Konig, M. Bolliger, M. Wieser, and H. Vallery, "Automation in rehabilitation: How to include the human into the loop," *World Congr. Med. Phys. Biomed. Eng.*, vol. 25, no. 13, pp. 180–183, 2009.

[2] Y. Liu and G. Nejat, "Robotic urban search and rescue: A survey from the control perspective," *J. Intell. Robot. Syst.*, vol. 72, no. 2, pp. 147–165, 2013.

[3] S. Hirche and M. Buss, "Human-oriented control for haptic teleoperation," *Proc. IEEE*, vol. 100, no. 3, pp. 623–647, Mar. 2012.

[4] Y. Li, K. Tee, S. S. Ge, and H. Li, "Building companionship through human-robot collaboration," in *Social Robotics* (Lecture Notes in Computer Science), vol. 8239, G. Herrmann, M. Pearson, A. Lenz, P. Bremner, A. Spiers, and U. Leonards, Eds. New York, NY, USA: Springer, 2013, pp. 1–7.

[5] V. Duchaine and C. Gosselin, "Safe, stable and intuitive control for physical human-robot interaction," in *Proc. IEEE Int. Conf. Robot. Autom.*, Kobe, Janan, 2009, pp. 3676–3681.

[6] S. S. Ge, C. Yang, Y. Li, and T. H. Lee, "Decentralized adaptive control of a class of discrete-time multi-agent systems for hidden leader following problem," in *Proc. IEEE/RSJ Int. Conf. Intell. Robots Syst.*, St. Louis, MO, USA, Oct. 11–15, 2009, pp. 5065–5070.

[7] Y. Yamamoto and X. Yun, "Effect of the dynamic interaction on coordinated control of mobile manipulators," *IEEE Trans. Robot. Autom.*, vol. 12, no. 5, pp. 816–824, Oct. 1996.

[8] R. Chipalkatty, G. Droge, and M. B. Egerstedt, "Less is more: Mixed-initiative model-predictive control with human inputs," *IEEE Trans. Robot.*, vol. 29, no. 3, pp. 695–703, Jun. 2013.

[9] N. Hogan, "Impedance control: An approach to manipulation—Part I: Theory; Part II: Implementation; Part III: Applications," *J. Dyn. Syst. Meas. Control*, vol. 107, no. 1, pp. 1–24, 1985.

[10] Y. Li and S. S. Ge, "Human-robot collaboration based on motion intention estimation," *IEEE/ASME Trans. Mechatronics*, vol. 19, no. 3, pp. 1007–1014, Jun. 2014.

[11] H. Wang and K. Kosuge, "Attractor design and prediction-based adaption for a robot waltz dancer in physical human-robot interaction," in *Proc. 10th World Congr. Intell. Control Autom.*, 2012, pp. 3810–3815.

[12] A. Tobergte, R. Konietschke, and G. Hirzinger, "Planning and control of a teleoperation system for research in minimally invasive robotic surgery," in *Proc. IEEE Int. Conf. Robot. Autom.*, 2009, pp. 4225–4232.

[13] G. Aguirre-Ollinger, J. E. Colgate, M. A. Peshkin, and A. Goswami, "Active-impedance control of a lower-limb assistive exoskeleton," in *Proc. 10th IEEE Int. Conf. Rehabil. Robot.*, 2007, pp. 188–195.

[14] M. S. Erden and B. Maric, "Assisting manual welding with robot," *Robot. Comput.-Integr. Manuf.*, vol. 27, pp. 818–828, 2011.

[15] K. P. Tee, R. Yan, and H. Li, "Adaptive admittance control of a robot manipulator under task space constraint," in *Proc. IEEE Int. Conf. Robot. Autom.*, 2010, pp. 5181–5186.

[16] M. Kimmel, M. Lawitzky, and S. Hirche, "6D workspace constraints for physical human-robot interaction using invariance control with chattering reduction," in *Proc. IEEE/RSJ Int. Conf. Intell. Robots Syst.*, Oct. 2012, pp. 3377–3383.

[17] J. Jiang and A. Astolfi, "Shared-control for fully actuated linear mechanical systems," in *Proc. IEEE Annu. Conf. Decision Control*, Dec. 2013, pp. 4699–4704.

[18] N. Jarrasse, V. Sanguineti, and E. Burdet, "Slaves no longer: Review on role assignment for human-robot joint motor action," *Adaptive Behav.*, vol. 22, no. 1, pp. 70–82, 2014.
[19] Z. Wang, A. Peer, and M. Buss, "An hmm approach to realistic haptic human-robot interaction," in *Proc. 3rd Joint Eurohaptics Conf. Symp. Haptic Interfaces Virtual Environ. Teleoperator Syst.*, 2009, pp. 374–379.
[20] P. Evrard and A. Kheddar, "Homotopy switching model for dyad haptic interaction in physical collaborative tasks," in *Proc. 3rd Joint EuroHaptics Conf. Symp. Haptic Interfaces Virtual Environ. Teleoperator Syst.*, Salt Lake City, UT, USA, 2009, pp. 45–50.
[21] P. Evrard and A. Kheddar, "Homotopy-based controller for physical human-robot interaction," in *Proc. 18th IEEE Int. Symp. Robot Human Interact. Commun.*, Sep. 2009, pp. 1–6.
[22] A. Mortl, M. Lawitzky, A. Kucukyilmaz, M. Sezgin, C. Basdogan, and S. Hirche, "The role of roles: Physical cooperation between humans and robots," *Int. J. Robot. Res.*, vol. 31, no. 13, pp. 1656–1674, 2012.
[23] J. R. Medina, M. Lawitzky, A. Molin, and S. Hirche, "Dynamic strategy selection for physical robotic assistance in partially known tasks," in *Proc. IEEE Int. Conf. Robot. Autom.*, 2013, pp. 1180–1186.
[24] J. R. Medina, D. Lee, and S. Hirche, "Risk-sensitive optimal feedback control for haptic assistance," in *Proc. IEEE Int. Conf. Robot. Autom.*, 2012, pp. 1025–1031.
[25] M. Saida, J. R. Medina, and S. Hirche, "Adaptive attitude design with risk-sensitive optimal feedback control in physical human-robot interaction," in *Proc. 21st IEEE Int. Symp. Robot Human Interactive Commun.*, Paris, France, Sep. 2012, pp. 955–961.
[26] N. Jarrasse, T. Charalambous, and E. Burdet, "A framework to describe, analyze and generate interactive motor behaviors," *PLoS ONE*, vol. 7, no. 11, p. e49945, 2013.
[27] S. P. Buerger, "Stable, high-force, low-impedance robotic actuators for human-interactive machines," Ph.D. dissertation, Department of Mechanical Engineering, Massachusetts Institute of Technology, Cambridge, MA, USA, 2005.
[28] S. S. Ge, Y. Li, and C. Wang, "Impedance adaptation for optimal robot-environment interaction," *Int. J. Control*, vol. 87, no. 2, pp. 249–263, 2014.
[29] T. Shima and S. Rasmussen, Eds. (2009). *UAV Cooperative Decision and Control*. Philadelphia, PA, USA: Society for Industrial and Applied Mathematics. [Online]. Available: http://epubs.siam.org/doi/abs/10.1137/1.9780898718584
[30] G. Hudas, K. G. Vamvoudakis, D. Mikulski, and F. L. Lewis, "Online adaptive learning for team strategies in multi-agent systems," *J. Defense Modeling Simul.: Appl. Methodology, Technol.* vol. 9, no. 1, pp. 59–69, 2012.
[31] T. Basar and G. J. Olsder. (1998). *Dynamic Noncooperative Game Theory*. 2nd ed. Philadelphia, PA, USA: Society for Industrial and Applied Mathematics. [Online]. Available: http://epubs.siam.org/doi/abs/10.1137/1.9781611971132
[32] C. Yang, G. Ganesh, S. Haddadin, S. Parusel, A. Albu-Schaeffer, and E. Burdet, "Human-like adaptation of force and impedance in stable and unstable interactions," *IEEE Trans. Robot.*, vol. 27, no. 5, pp. 918–930, Oct. 2011.
[33] J. E. Slotine and W. Li, *Applied Nonlinear Control*. Englewood Cliff, NJ, USA: Prentice-Hall, 1991.

Yanan Li (S'10–M'14) received the B.Eng. degree in control science and engineering and the M.Eng. degree in control and mechatronics engineering from Harbin Institute of Technology, Harbin, China, in 2006 and 2009, respectively, and the Ph.D. degree from NUS Graduate School for Integrative Sciences and Engineering, National University of Singapore, Singapore, in 2013.

He is a Research Scientist with the Institute for Infocomm Research, Agency for Science, Technology and Research (A*STAR), Singapore. His research interests include physical human–robot interaction, human–robot shared control, and control theory and applications.

Keng Peng Tee (S'04–M'08) received the B.Eng (first class hons.) and M.Eng degrees in mechanical engineering, and the Ph.D. degree in electrical and computer engineering, in 2001, 2003, and 2008, respectively, all from National University of Singapore.

In 2008 he joined the Institute for Infocomm Research, Agency for Science, Technology and Research (A*STAR), Singapore, where he is now a Group Leader. He has been an Associate Editor for the Conference Editorial Board of the IEEE Control Systems Society since 2012. His research interests include control of adaptive control, robot manipulation, human–robot interfaces, and human–robot collaboration.

Dr. Tee received the Godfrey Rajasooria Silver Medal in 2001, the A*STAR Graduate Scholarship from 2004–2008, and the IES Prestigious Engineering Award in 2009.

Wei Liang Chan received the B.S. degree in electrical engineering from National University of Singapore, Singapore, in 2011.

He is a Research Engineer with the Institute for Infocomm Research, Agency for Science, Technology and Research (A*STAR), Singapore. His research interests include human–robot interaction, telerobotic systems, and user interface design for robotics.

Rui Yan (M'11) received the B.S. and M.S. degrees from the Department of Mathematics, Sichuan University, Chengdu, China, in 1998 and 2001, respectively, and the Ph.D. degree from the Department of Electrical and Computer Engineering, National University of Singapore, Singapore, in 2006.

She is a Research Scientist with the Institute for Infocomm Research, Agency for Science, Technology and Research (A*STAR), Singapore. Her research interests include intelligent robots, nonlinear control, neural computation, and power systems analysis.

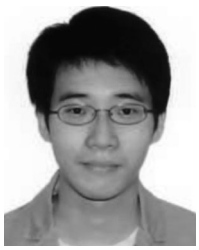

Yuanwei Chua received the B.S. degree in mechanical engineering and the M.S. degree in electrical engineering from National University of Singapore, Singapore, in 2009 and 2013, respectively.

He is a Research Engineer with the Institute for Infocomm Research, Agency for Science, Technology and Research (A*STAR), Singapore. His research interests include bimanual manipulation and interactive multimodal robot behavior.

Dilip Kumar Limbu received the B.Sc. degree in computer science and the M.Sc. degree (with distinction) in information technology for manufacture from The Coventry University, Coventry, U.K., in 1997 and 1998, respectively. He received the Ph.D. degree from the School of Computing and Mathematical Sciences, Auckland University of Technology, Auckland, New Zealand.

Since 2008 he has been a Scientist with the Institute for Infocomm Research, Agency for Science, Technology and Research (A*STAR), Singapore. He was an Associate Research Fellow and Research Engineer with the Singapore Institute of Manufacturing Technology, Singapore from 2000 to 2004. He has more than 15 years of experience in research and development in robotics and information retrieval.